JACS
JOURNAL OF THE AMERICAN CHEMICAL SOCIETY
Article
pubs.acs.org/JACS

Mineral Formation in the Larval Zebrafish Tail Bone Occurs via an Acidic Disordered Calcium Phosphate Phase

Anat Akiva,[†,⊥] Michael Kerschnitzki,[†,⊥] Iddo Pinkas,[‡] Wolfgang Wagermaier,[§] Karina Yaniv,[∥] Peter Fratzl,[§] Lia Addadi,[*,†] and Steve Weiner[†]

[†]Department of Structural Biology, Weizmann Institute of Science, Rehovot 76100, Israel
[‡]Department of Chemical Research Support, Weizmann Institute of Science, Rehovot 76100, Israel
[§]Department of Biomaterials, Max Planck Institute of Colloids and Interfaces, 14476 Potsdam, Germany
[∥]Department of Biological Regulation, Weizmann Institute of Science, Rehovot76100, Israel

ABSTRACT: Both *in vivo* and *ex vivo* observations support the hypothesis that bone mineral formation proceeds via disordered precursor phases. The characteristics of the precursor phases are not well defined, but octacalcium phosphate-like, amorphous calcium phosphate-like, and HPO_4^{2-}-enriched phases were detected. Here we use *in vivo* Raman spectroscopy and high-resolution wide-angle X-ray diffraction (WAXD) to characterize and map at 2 μm resolution the mineral phases in the rapidly forming tail fin bones of living zebrafish larvae and zebrafish larvae immediately after sacrifice, respectively. Raman spectroscopy shows the presence of an acidic disordered calcium phosphate phase with additional characteristic features of HPO_4^{2-} at the bone−cell interface. The complexity in the position and shape of the ν_1 PO_4 peak viewed by *in vivo* Raman spectroscopy emphasizes the heterogeneity of the mineral during bone formation. WAXD detects an additional isolated peak, appearing alone or together with the characteristic diffraction pattern of carbonated hydroxyapatite. This unidentified phase is located at the interface between the mature bone and the surrounding tissue, similar to the location at which the disordered phase was observed by Raman spectroscopy. The variable peak positions and profiles support the notion that this is an unstable disordered precursor phase, which conceivably crystallized during the X-ray diffraction measurement. Interestingly, this precursor phase is co-aligned with the *c*-axes of the mature bone crystals and thus is in intimate relation with the surrounding collagen matrix. We conclude that a major disordered precursor mineral phase containing HPO_4^{2-} is part of the deposition pathway of the rapidly forming tail fin bones of the zebrafish.

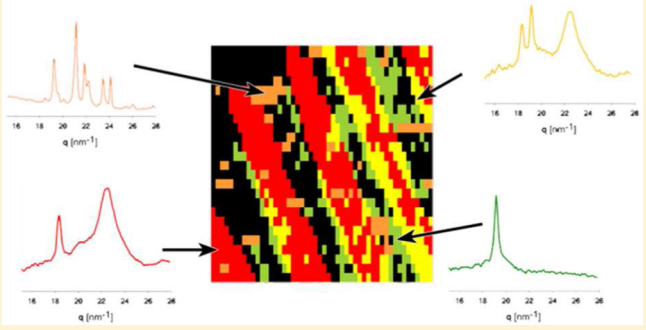

INTRODUCTION

Many biological minerals form via highly disordered precursor phases.[1−10] In the case of the mature carbonated hydroxyapatite mineral phase of bone, the involvement of a crystalline octacalcium phosphate (OCP, $Ca_8H_2(PO_4)_6{\cdot}5H_2O$) precursor phase was first suggested in 1957 by Brown and colleagues.[11] They also suggested that the sequence of events leading to apatite formation in bone is $CaHPO_4{\cdot}2H_2O \rightarrow$ OCP $\rightarrow$ apatite. In 1966, Termine and Posner showed by IR analysis of rat bone that amorphous calcium phosphate (ACP) is more abundant in the early stages of bone formation.[12]

Direct *in vivo* evidence for the existence of this phase, or other suggested precursor phases, was obtained in 2006, when Crane et al. performed a Raman microspectroscopy (μ-Raman spectroscopy) analysis of the forming suture of mice calvaria.[13] They showed that the predominant mineral precursor phase in the suture was an OCP-like phase, with the possibility that an ACP phase was also present. Mahamid et al.[14] used wide-angle X-ray diffraction (WAXD) to examine freshly dissected adult zebrafish tails that were immediately rinsed in acetone for rapid dehydration in order to prevent crystallization. A broad diffraction peak corresponding to a disordered ACP phase was observed. Peak fitting showed that this broad peak centered at q = 19.4 nm^{-1} (d spacing = 3.23 Å), rather than at q = 23 nm^{-1} (d spacing = 2.98 Å), as was previously reported for synthetic ACP that originated from tricalcium phosphate.[15,16] A sharper peak centered at 19.4 nm^{-1} also appeared together with the peaks of carbonated hydroxyapatite (cHAP), and was thought to be an artifact. Using transmission electron microscopy and energy-dispersive X-ray spectroscopy, Mahamid et al. determined a Ca/P ratio of 0.75 ± 0.22[17] in intracellular mineral-containing vesicles in embryonic mice calvaria, raising the possibility that calcium polyphosphates are present in the mineral vesicles.[18] Recently, μ-Raman spectroscopy, performed *in vivo* on maturing bone minerals in the larval zebrafish tail fin, showed the coexistence of cHAP with a disordered OCP-like phase. Weak absorptions of HPO_4^{2-} species were also observed.[19]

Received: September 8, 2016
Published: October 6, 2016

DOI: 10.1021/jacs.6b09442
J. Am. Chem. Soc. 2016, 138, 14481−14487

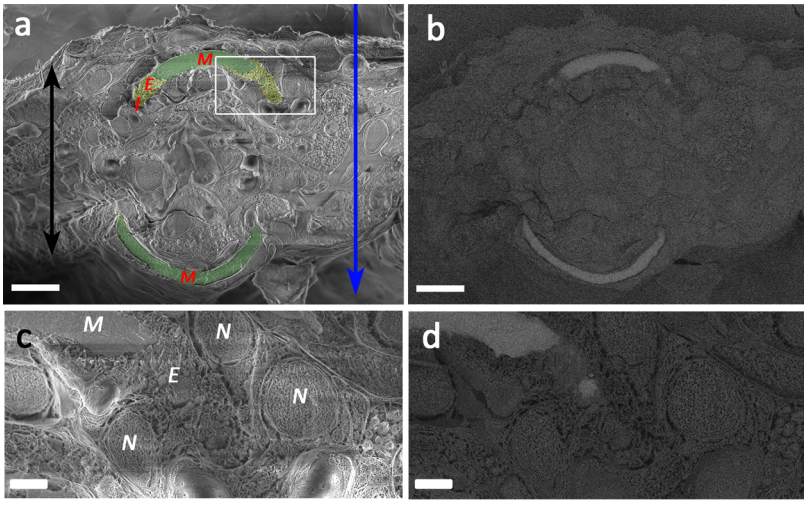

Figure 1. Cryo-SEM micrographs of a zebrafish bony ray in cross section. (a) In-lens image showing the mineralized bone (green, M), the bone edges (non-mineralized collagen, yellow, E), and the bone–cell interface (I). Each ray is growing both toward the distal part of the tail (perpendicular to the image plane) and toward the edges of each ray, where the non-mineralized collagen is observed (yellow, E). The black arrow spans the tissue boundaries. The μ-Raman and μ-WAXD beams illuminate the tissue in the direction of the blue arrow. (b) Back-scattered electron (BSE) micrograph of (a), showing the electron-dense material of the bone. (c) Higher magnification of the non-mineralized region and the bone–cell interface shown in (a) (white rectangle). (d) BSE micrograph of (c), showing new mineralization sites at the bone edge. M, mature bone; E, bone edge; N, nucleus. Scale bars: (a,b) 10 μm and (c,d) 2 μm.

Spevak et al.[20] used Fourier transform infrared spectroscopic imaging of developing bones (bovine, baboon, and mouse bones) to show that the younger regions have larger amounts of acid phosphate (HPO_4^{2-}).

Using ^{31}P NMR on bones from different animals, Wu et al.[21] observed signals from HPO_4^{2-} in early stages of bone formation, in a hybrid structure between brushite (dicalcium hydrogen phosphate dehydrate, $CaHPO_4{\cdot}2H_2O$, also called DCPD) and OCP phases. Later, the same authors suggested that organic phosphate is a major component in the early stages of bone formation.[22] It is interesting to note that all the above FTIR, Raman, and NMR spectroscopy show the presence of HPO_4^{2-} in an undefined structure in maturing bone, but not in mature bone.[19−21,23]

Francis and Webb formulated a hypothesis whereby cHAP matures from brushite, which has a ratio of Ca/P = 1. Rapid deposition of a disordered brushite phase would be followed by slow transformation into apatite.[24] Habraken et al. showed that, under controlled calcium concentrations and pH conditions, ACP is formed by association of $Ca_2(HPO_4)_3^{2-}$ clusters at pH 7.2.[25]

The challenge involved in identifying and characterizing highly unstable precursor phases in biological environments is that any perturbation during sample preparation and analysis may change the phase and result in an artifact. Rapid time evolution, drying, acidification of the environment following cell death, heating, and high-energy irradiation all have the potential to cause phase transformations. Every technique has its own pitfalls: therefore, only coordinated observations using multiple techniques *in vivo*, or in tissues preserved as close as possible to physiological conditions, can provide information on the *in vivo* precursor mineral forms. For lack of a better word, we shall continue to address these disordered mineral forms as "phases", although we are aware that they cannot be truly called a "phase", because they are not well defined in either composition or structure.

The tail fin bones of the zebrafish larva are a good model for studying bone precursor phases because bone formation is rapid.

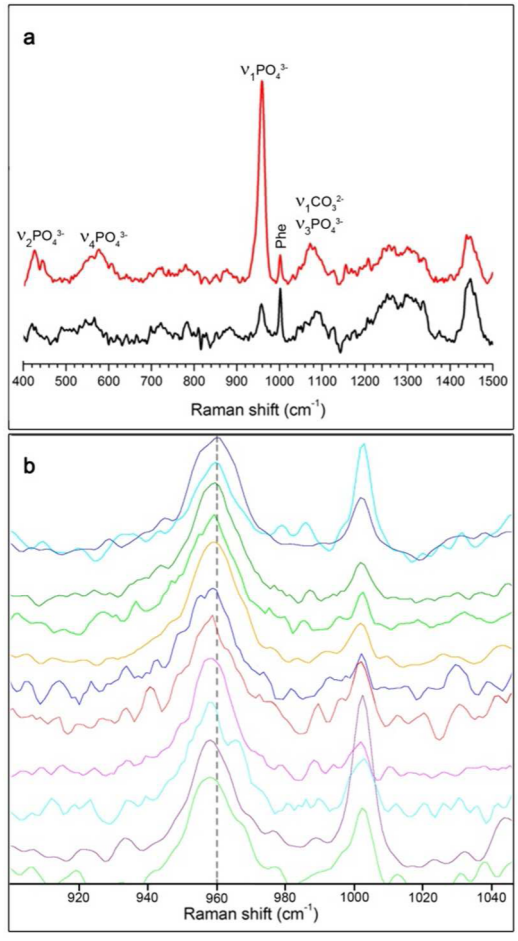

Figure 2. (a) μ-Raman spectra of zebrafish tail bones acquired on living fish: mature bone (red) and bone edge (black). (b) Raman spectra from a series of bone edges, showing a shift of the ν_1 peak from 960 cm^{-1} (dashed line) to lower wavenumbers. The spectral intensities were normalized to the main ν_1 PO_4^{3-} peak and the position to the Phe peak at 1003 cm^{-1}.

DOI: 10.1021/jacs.6b09442
J. Am. Chem. Soc. 2016, 138, 14481−14487

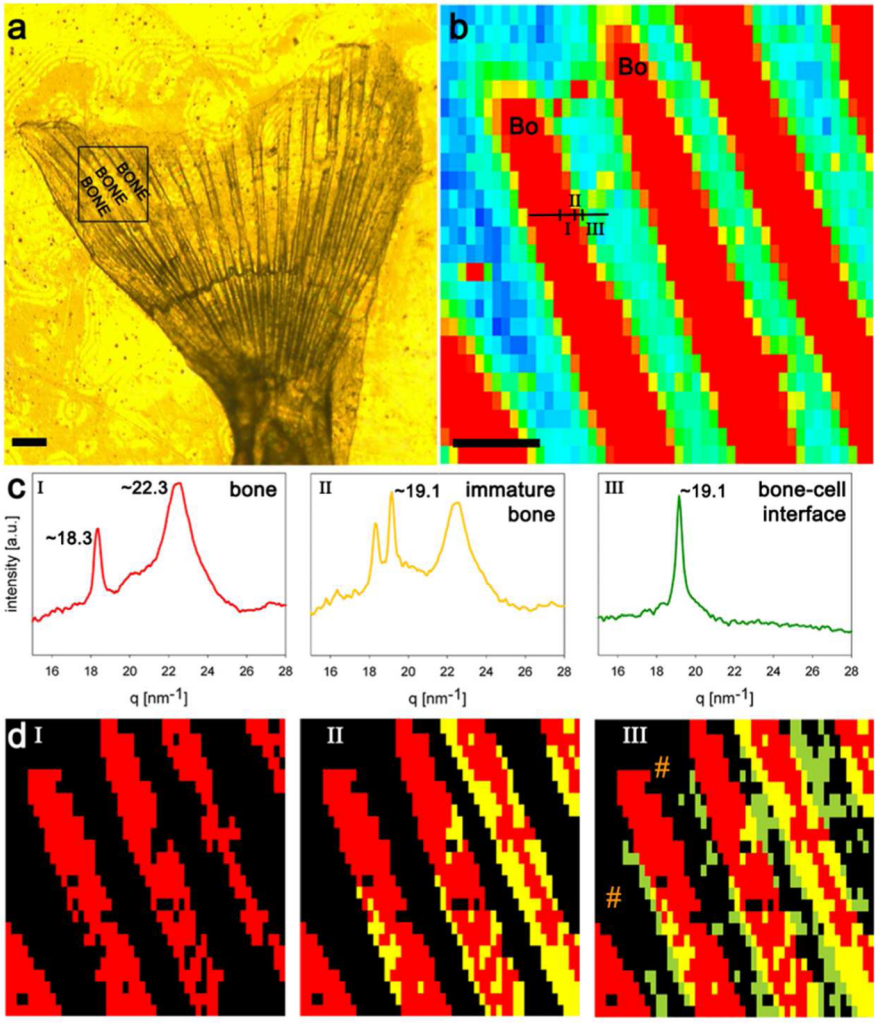

Figure 3. Zebrafish caudal fin and mineral distribution: (a) Light microscopy image of 30 dpf zebrafish tail mounted on a kapton foil just before the X-ray measurement. (b) X-ray fluorescence (XRF) map of the calcium distribution in the caudal fin showing the mineralized zebrafish tail bones (Bo = bone) embedded in the soft tissue (color code of Ca XRF: red = calcium rich, blue = calcium poor). Note the presence of calcium-rich aggregate regions (yellow and red) between the bone structures. (c) WAXD patterns measured at different locations of a ray (indicated by I–III in the XRF map in (b)), showing mature bone (I), immature bone (II), and the bone–cell interface (III). Mature bone mineral is characterized by the hydroxyapatite (002) diffraction at q = 18.3 nm^{-1} and the unresolved (211), (112), and (300) diffractions at q = 22.3 nm^{-1}. In the transition zone between the bone structures and the soft tissue, a diffraction peak appears at q = 19.1 nm^{-1}. (d) Classification of different mineral phases. The scanned area is the same as in (b); and the color code corresponds to the diffraction pattern in (c): red, HAP, diffraction I; yellow, HAP + the additional diffraction peak at q = 19.1 nm^{-1}, diffraction II; green, diffraction peak at q = 19.1 nm^{-1}, diffraction III. The # symbols mark the positions of the calcium-rich aggregates between the bones in the XRF image. Pixel resolution is 2 μm in a total scanned region of 100 × 100 μm.

The bones are small (hundreds of micrometers wide and only 1–2 μm in thickness, see Figure 1), and the very thin tissue in which they are embedded (20–50 μm) allows direct access to bone mineral *in vivo*[19,26] (Figure 1a,c). Here we use μ-spot confocal Raman spectroscopy and fast synchrotron WAXD to monitor bone development. Confocal μ-Raman spectroscopy is performed on living fish. WAXD with a 2 μ-spot X-ray beam is used to rapidly scan freshly dissected tail fin bones from regions covering mature bone (proximal tail) to newly formed regions (distal tail).

RESULTS

In Vivo Raman Spectroscopy of Newly Formed Bones.

We used μ-Raman spectroscopy to obtain information on the mineral composition of the tail fin bone of living zebrafish larvae 25–30 days post fertilization (dpf). The bones are ~30 μm wide and 1–2 μm thick. The bone surface was scanned from the center of the ray (Figure 1a, M) toward the bone-cell interface (Figure 1a, I) with a 2 μm spot size. Four separate measurements were performed for each section. The bone edge was defined as the last spectrum showing mineral before the detection of only soft tissue. The mature bone mineral (Figure 2) produces a typical Raman bone spectrum of cHAP, with the main ν_1 PO_4^{3-} peak located at 960 cm^{-1}. The ν_2 PO_4^{3-} and ν_4 PO_4^{3-} are well separated and are located at 425 and 580 cm^{-1}, respectively.[27,28] Based on the ratio between the ν_1 PO_4^{3-} peak intensity and the phenylalanine (Phe) peak at 1003 cm^{-1}, the Raman spectrum of the bone edge shows a major decrease in mineral content. Shifts to lower wavenumbers are observed for the ν_2 PO_4^{3-} and ν_4 PO_4^{3-} vibrational modes (420 and 560 cm^{-1}, respectively) relative to the mature bone. A broad peak is also observed between the ν_2 PO_4^{3-} and ν_4 PO_4^{3-} peaks at 500 cm^{-1}. We were not able to characterize the vibrational modes associated with

DOI: 10.1021/jacs.6b09442
J. Am. Chem. Soc. 2016, 138, 14481–14487

this peak. The shift to lower wavenumbers of the ν_2 PO_4^{3-} and ν_4 PO_4^{3-} are attributed to the presence of an acidic ACP phase.[19] We collected many bone edge spectra and examined the ν_1 PO_4^{3-} peak shapes in detail (Figure 2b). The strongest ν_1 PO_4^{3-} peak positions vary between 957.7 and 960.3 cm^{-1}. A Raman shift of the ν_1 PO_4^{3-} peak to lower wavenumbers (e.g., 957 cm^{-1}) is consistent with immature bone containing extensive amounts of HPO_4^{2-}.[13,29,30] The ν_1 PO_4^{3-} peaks also have complex shapes, due to the presence of different mineral components of diverse compositions (Figure 2b). In some spectra, a shoulder appears at ~955 cm^{-1}, whereas in others a shoulder is observed at ~966 cm^{-1}. The intensity of the Phe peak located at 1003 cm^{-1} can be used as an indication of overall organic content at the edge. We did not detect, however, any correlation between the position and intensity of the main ν_1 PO_4^{3-} peak and the Phe peak intensity (Figure 2b).

Wide-Angle X-ray Diffraction of Zebrafish Tail Bones. In order to obtain more insight into the nature and distribution of the immature mineral phase(s) that was detected by Raman spectroscopy at the bone edge, we used high-resolution (2 μm) X-ray measurements on zebrafish larvae at the stage 25−30 dpf. The zebrafish larvae were sacrificed a few minutes prior to the X-ray measurements and the tail bones and intervening tissues were immediately measured without any sample treatment (Figure 3a). A whole tail screening requires <30 min, and the energy of the beam is 14 keV.

The calcium X-ray fluorescence (XRF) map clearly shows the bone locations, as well as the presence of some Ca-rich areas between the bones (Figure 3b). The WAXD patterns are used to map the spatial distributions of different minerals. Whereas the developed bone shows a typical diffraction pattern of HAP (Figures 3c-I, d red), an additional peak (Figure 3c-II) is obtained from the bone edge (Figure 3b-II, d yellow). The mature bone pattern (red), the mixed diffraction pattern (yellow), and the single additional peak pattern (green) often appear in a specific spatially discrete sequence (Figure 3d-III). The additional peak is centered at q = 19.1 nm^{-1}. At several locations, the same diffraction peak is present, without the peaks from the apatite diffraction pattern (Figure 3c-III). These single peak diffraction patterns are clearly located at the outermost edge of the bone rays close to the interface with the soft tissue, (Figure 3b-III, d green). This is essentially the same location from which the Raman spectra of the edge were obtained. Thus, both Raman and X-ray mapping confirm the presence of a different mineral phase at the edges of the tail bones; the location where the most recently formed bone mineral is located.

The additional peak (Figure 3c-II) centered at q = 19.1 nm^{-1} varies in intensity relative to the (002) diffraction of HAP (Figure 4a). Some of the peak profiles of the same peak detected individually are even more complex than those observed together with HAP (Figure 4b, e.g., black profile). Interestingly, the full width at half-maximum (fwhm) values of the (002) peak of HAP and of the additional peak at q = 19.1 nm^{-1} are 0.366 and 0.394, respectively. This similarity in width highlights the fact that the two mineral phases are both poorly crystalline.

The WAXD patterns of the developed HAP bone mineral consist of two main diffraction rings (Figure 5a, left). The inner ring corresponds to the HAP (002) diffraction at $q \approx 18.3$ nm^{-1} and the outer ring corresponds to the unresolved (112), (211) and (300) diffraction peaks around q = 22.3 nm^{-1}. WAXD patterns that derive from the bone-cell interface (region III in Figure 3), consisting of one ring located at $q \approx 19.1$ nm^{-1} (Figure 5a, right), clearly differ from both HAP diffraction

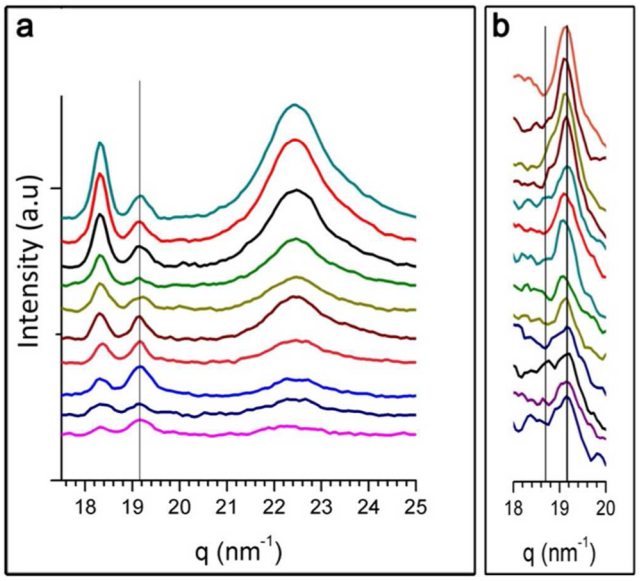

Figure 4. (a) WAXD patterns showing variations in the additional peak position and relative intensity of the immature bone region of different bone rays where HAP was also present (Figure 3c-II). The black vertical line is at q = 19.1 nm^{-1}. (b) The immature bone region at locations where only the unknown phase is present (Figure 3c-III). The black lines mark the region q = 18.7−19.15 nm^{-1}.

positions and can thus be followed individually. In most frames, the azimuthal distribution shows preferred orientation parallel to that of the HAP (002) diffraction (Figure 5a,b). Plotting the azimuthal profile of the HAP (002) diffraction and of the additional peak from all scan frames (total of 1300 points) reveals that the two mineral phases are indeed co-aligned over whole bone segments (Figure 5c).

Some locations within the soft tissue between bones gave high Ca XRF signals (Figures 3b and 6a,b). Note that intracellular calcium-rich particles were detected between the bones by *in vivo* confocal microscopy.[26] A considerable number of diffraction patterns (>40) were obtained from the locations with high Ca XRF signals. These patterns derive from polycrystalline material with crystals slightly different from each other in orientation, relative intensities and diffraction positions, even at neighboring scan locations (Figure 6c, green and red, and 6b, arrowhead). As these diffraction patterns contain many reflections, the nature of the crystalline phase can be defined. The only reasonable match that we could find between these diffraction patterns and those of the known calcium phosphate crystalline phases was to a mineral phase that contains diffraction features of both crystalline monetite (DCPA, $CaHPO_4$) and brushite (DCPD, $CaHPO_4{\cdot}2H_2O$) (Figure 6d). This crystalline phase is not β-TCP or OCP (note the absence of the two prominent peaks of OCP around q = 7 nm^{-1}, Figure 6d).

DISCUSSION

Here we show the presence of non-apatitic mineral phases at the bone edge, namely at the bone-cell interface. Raman microspectroscopy performed on living fish and high-resolution X-ray diffraction (WAXD) mapping performed on freshly dissected tails, confirm that bone mineralization proceeds through a transient mineral phase or phases. Although this transient mineral phase is clearly complex, some features are common to both analyses.

Raman Microspectroscopy. *In vivo* characterization of the non-apatitic mineral phase at the bone edge shows variations in

DOI: 10.1021/jacs.6b09442
J. Am. Chem. Soc. 2016, 138, 14481−14487

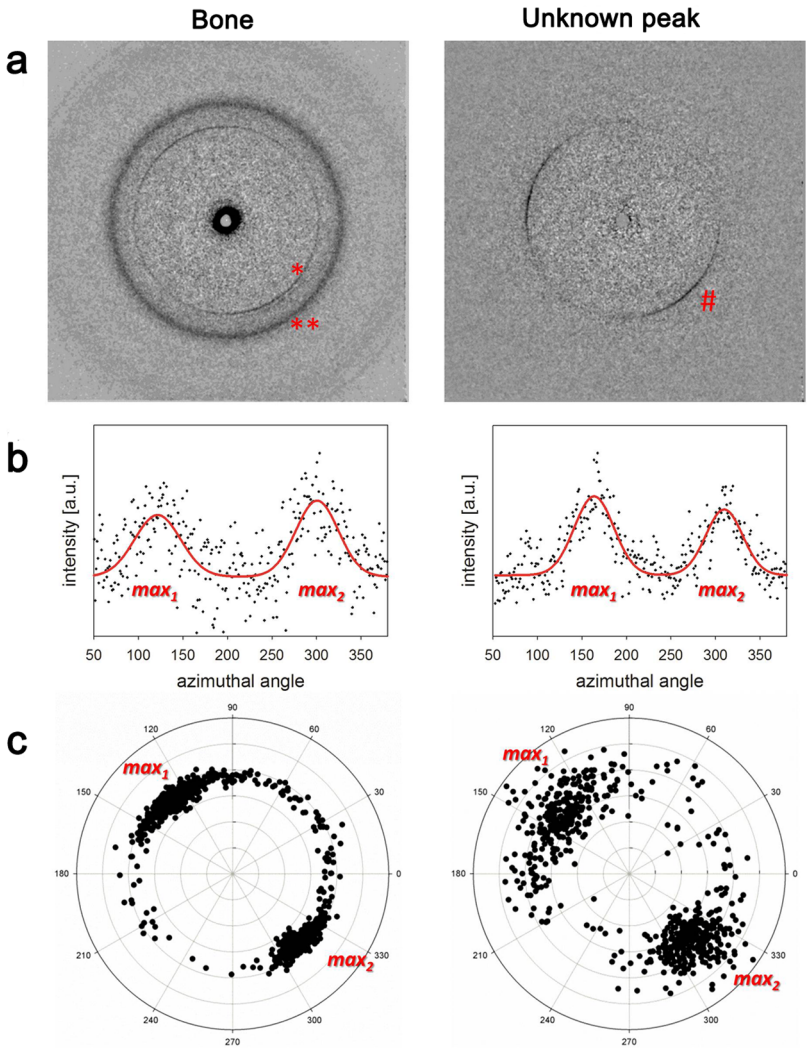

Figure 5. Mineral orientation. (a) WAXD: left, bone (*, (002); **, (112), (211), and (300) of carbonated hydroxyapatite); right, # unknown peak. (b) Azimuthal integration of the diffractograms in (a) showing the diffraction intensities relative to the azimuthal angle. Azimuthal angles with maximum intensity indicate the preferred orientation of the diffraction peaks. (c) Polar plot of the azimuthal maximum positions of 1300 diffractograms collected over a wide region of the tail. The radial axis depicts the fwhm of the respective peak derived from the radial integration. Note that bone apatite and the unknown mineral show similar preferred orientations.

the peak position and complexity of the ν_1 PO_4 absorption peak. The peak position around 957 cm^{-1} indicates that a major component of the edge mineral is a disordered CaP phase that is enriched in HPO_4^{2-}.[13,29,30] The shoulders that are observed on both sides of the main Raman peak, namely at 955 and 966 cm^{-1} can be attributed both to ACP and to OCP-like phases.[13,27,28] In addition, the ν_4 PO_4 peak is located at lower wavenumbers relative to HAP and OCP. This also indicates the presence of acidic ACP enriched by HPO_4^{2-}.

The presence of HPO_4^{2-} in immature bone was previously shown in different types of bone using different spectroscopic methods, including ^{31}P NMR, FT-IR, and Raman spectroscopy.[20,21,23] A previous *in vivo* Raman spectroscopy study of zebrafish fin bones also showed the presence of HPO_4^{2-}.[19] This was thought to be related to ACP precipitated from an acidic environment, or to HPO_4 stretching modes of an OCP-like phase. Some of the studies related the presence of HPO_4^{2-} to an OCP-like phase.[13,27] We conclude from these Raman measurements, that the detected HPO_4^{2-} in the living fish tail originate from an acidic ACP with large amounts of HPO_4^{2-}. The detection of different phases such as acidic ACP and OCP-like phases at the same location or separately at the bone edges, probably indicates the existence of a transient disordered phase that undergoes fast transformation, possibly even induced by the measurement itself.

X-ray Diffraction. A non-apatitic mineral phase is detected by WAXD at the bone edges. This phase is poorly crystalline, and is characterized by a composite diffraction peak centered at $q \approx 19$ nm^{-1}. This non-apatitic phase being crystalline is inconsistent with the Raman observations of a disordered phase, but both appear in the same locations, where new bone mineral is deposited. We suspect that the measurement conditions may have induced an initially noncrystalline phase to crystallize.

The crystallization most likely took place after the disordered phase had infiltrated into the collagen. This we infer from the observation that the crystalline phase has preferred orientation, and that this orientation is aligned with the orientations of the cHAP crystals in the mature bone. The latter are aligned with the collagen fibril axes.

We did observe that mineral in the soft tissue between the bones but at considerable distance from them produced a complex crystalline diffraction pattern that corresponds to a

DOI: 10.1021/jacs.6b09442
J. Am. Chem. Soc. 2016, 138, 14481−14487

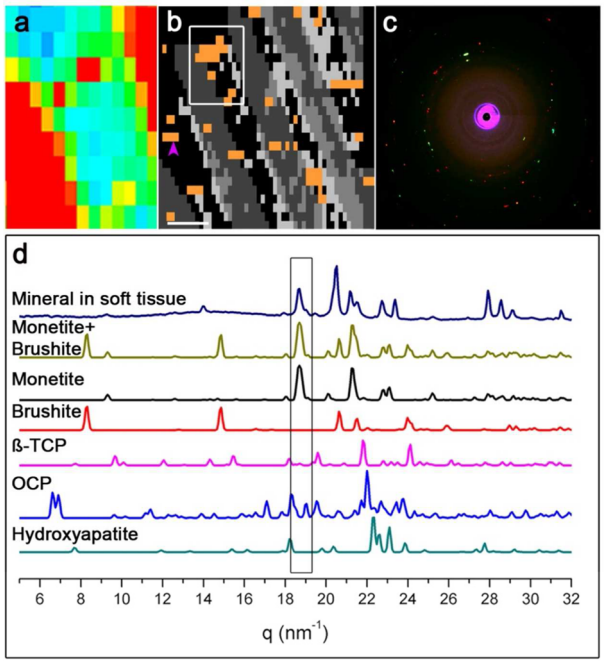

Figure 6. Crystalline mineral WAXD patterns. (a) Calcium XRF map of the region marked by the rectangle in (b), showing high Ca content between different bones. The crystalline material appears mainly between bones and at the distal part of the bone ray. Color code: blue to red indicates increasing calcium concentrations. (b) 2D grayscale map of mineral distribution as was described in Figure 3d. The additional orange color shows the locations of the non-apatitic crystalline material. (c) Projection of two adjacent WAXD micrographs of crystalline materials (green and red). The location of the two adjacent WAXD patterns are designated by an arrowhead in (b). (d) Comparison of one integrated diffraction pattern of crystalline mineral in soft tissue with the pattern of synthetic CaP minerals, obtained from the Inorganic Crystal Structure Database (ICSD) (collection codes: 2745, 16132, 97500, 27050, 289993).

mixture of monetite and brushite. An earlier study also using Raman spectroscopy did not identify crystalline deposits in this tissue, but did identify ACP and OCP-like phases.[26] So here too the crystallinity is an artifact, but we can infer that the original disordered phase may have been enriched in HPO_4^{2-}, as monetite and brushite are both acidic phases. Note that stability field diagrams show that monetite, brushite, OCP and TCP at millimolar concentrations are all stable within a fairly narrow pH range (5.5–7).[16] It is therefore conceivable that different transient phases will be induced to form under the influence of slight external or intrinsic modifications of the environment.

We note that brushite, monetite, and acidic ACP all have Ca/P ratios equal to 1, and that a TEM study of mineral in the vesicles associated with mouse bone formation showed Ca/P ratios even below 1.[17] A recent study where ACP was synthesized *in vitro* under controlled conditions also yielded similar values.[17,25]

CONCLUSIONS

Both Raman spectroscopy and X-ray diffraction confirm the presence of a transient precursor mineral phase at the forming edges of the fin bone. The Raman spectroscopy in particular shows that a major component of this precursor phase is HPO_4^{2-}, leading us to conclude that the phase is an acidic disordered form of calcium phosphate. The fact that the transient precursor phase crystallizes with preferred orientation, aligned with the mature mineral, indicates that the precursor is in intimate contact with the collagen fibrils.

EXPERIMENTAL SECTION

Zebrafish Husbandry. Adult and larval zebrafish were raised and maintained as described[31] and were handled according to the guidelines of the Weizmann Institute Animal Care and Use Committee. Embryos were generated by natural spawning and raised in blue water in an incubator at 28 ± 0.5 °C as described.[32] Zebrafish nacre mutant "albino" fish[33] were used in order to avoid WAXD patterns and Raman fluorescence, which originate from pigment cells.

Cryo-SEM. Tails were dissected from 25–30 dpf zebrafish and were immersed immediately in 10% dextran (Fluka), sandwiched between two metal discs (3 mm diameter, 0.1 mm cavities with flat cover above), and cryoimmobilized in a high-pressure freezing device (HPM10; Bal-Tec). The frozen samples were removed from the cavity, mounted on a holder under liquid nitrogen, and transferred to a freeze fracture device (BAF 60; Bal-Tec) using a vacuum cryotransfer device (VCT 100; Bal-Tec). Samples were fractured at a temperature of −120 °C and then etched for 5 min at −105 °C at a vacuum better than 5×10^{-7} mbar. This preparation was used to generate a transverse view of the bones (Figure 1). Samples were observed in an Ultra 55 scanning electron microscope (Zeiss, Germany) by using a secondary electron in-lens detector and a backscattered electron in-lens detector (operating at 1 kV) in the frozen hydrated state by use of a cryostage at a temperature of −120 °C.

Raman Spectroscopy. The larvae were anesthetized with tricaine–methanesulfonate (MS 222) (0.12%), mounted on a microscope slide in water, and examined directly. At the end of the experiment, the fish were still alive and apparently in good conditions, as judged by their unimpaired ability to swim after recovering from the anesthesia.

Raman measurements were conducted on a LabRAM HR Evolution instrument (Horiba, Japan) configured with four laser lines (325, 532, 632, and 785 nm), allowing for Raman spectra from 50 cm^{-1} and onward. The instrument is equipped with an 850 mm spectrograph. The system's pixel spacing is 1.3 cm^{-1} when working with a 600 grooves/mm grating; it is also equipped with other gratings. The excitation and emission beams have the option of automatic rotation of the light polarization as well as a depolarizer in front of the spectrograph to eliminate polarization effects of the grating. The light is brought to the sample using various objectives (Olympus 100×, 50×, 10×, 50× LWD and 74× fully achromatic reflective objective). The LabRAM instrument is equipped with two detectors: a 1024 × 256 pixel open electrode front-illuminated CCD camera cooled to −60 °C and a 1600 × 200 pixel front-illuminated EMCCD camera cooled to −60 °C for fast scanning protocols. The system is set around an open confocal microscope (Olympus BX41) with a spatial resolution better than 1 μm using the 100× NA 0.9 objective. The sample is placed upon a motorized stage that can be software-controlled to measure Raman spectral maps of the samples. In order to find small targets on large areas, the instrument can scan areas using the Duo-Scan Galvo unit and the SWIFT protocol. Most of the work on this project was done using the 632.8 nm HeNe laser, the 600 grooves/mm grating, and the 100× objective.

Sample Preparation for X-ray Measurements. Larval zebrafish (25–30 days post fertilization) were sacrificed a few minutes before the measurement and were mounted under the binocular on a kapton foil inside a lead tape frame. The frame including the sample was clamped to an X-ray holder and magnetically fixed on a translational stage.

Xray Diffraction. Tail samples were scanned at the P03 beamline at the PETRA III storage ring at DESY, Hamburg, Germany, and at the Nanofocus beamline ID13 at the European Synchrotron Radiation Facility (ESRF), Grenoble, France, using a monochromatic 14-keV X-ray beam (λ = 0.886 Å) with a beam size of 2 μm. During scanning, the stage was translated perpendicularly to the beam with a step size of 2 μm. Typical scan areas had a dimension of 100 × 100 μm, including around 2500 recorded WAXD patterns for a full scan (total measurement time less than 30 min). The exposure time for each point was approximately 0.5 s. Simultaneously, the calcium XRF signal was

DOI: 10.1021/jacs.6b09442
J. Am. Chem. Soc. 2016, 138, 14481–14487

obtained with an XRF detector, which was situated approximately 20 mm behind the sample at an angle of 90° to the X-ray path. The X-ray data were analyzed with the DPDAK software package[34]

AUTHOR INFORMATION

Corresponding Author

*lia.addadi@weizmann.ac.il

Author Contributions

⊥A.A. and M.K. contributed equally to this work.

Notes

The authors declare no competing financial interest.

ACKNOWLEDGMENTS

We very much appreciate the granted beamtimes at the ESRF, France, and PETRAIII, Germany, and thank M. Burghammer and C. Krywka for their support. We thank Dr. W. Habraken for useful discussions. This research was supported in part by a German Research Foundation grant, within the framework of the Deutsch-Israelische Projektkooperation. M.K. is supported by a Minerva Foundation postdoctoral fellowship. L.A. is the incumbent of the Dorothy and Patrick Gorman Professorial Chair of Biological Ultrastructure, and S.W. is the incumbent of the Dr. Trude Burchardt Professorial Chair of Structural Biology.

REFERENCES

(1) Towe, K. M.; Lowenstam, H. A. *J. Ultrastruct. Res.* **1967**, *17*, 1.
(2) Lowenstam, H.; Weiner, S. *Science* **1985**, *227*, 51.
(3) Addadi, L.; Raz, S.; Weiner, S. *Adv. Mater.* **2003**, *15*, 959.
(4) Dillaman, R.; Hequembourg, S.; Gay, M. *J. Morphol.* **2005**, *263*, 356.
(5) Gago-Duport, L.; Briones, M.; Rodríguez, J.; Covelo, B. *J. Struct. Biol.* **2008**, *162*, 422.
(6) Weiner, S.; Mahamid, J.; Politi, Y.; Ma, Y.; Addadi, L. *Front. Mater. Sci. China* **2009**, *3*, 104.
(7) Beniash, E.; Metzler, R. A.; Lam, R. S.; Gilbert, P. *J. Struct. Biol.* **2009**, *166*, 133.
(8) Weiner, S.; Addadi, L. *Annu. Rev. Mater. Res.* **2011**, *41*, 21.
(9) DeVol, R. T.; Sun, C.-Y.; Marcus, M. A.; Coppersmith, S. N.; Myneni, S. C.; Gilbert, P. U. *J. Am. Chem. Soc.* **2015**, *137*, 13325.
(10) Hasse, B.; Ehrenberg, H.; Marxen, J. C.; Becker, W.; Epple, M. *Chem. - Eur. J.* **2000**, *6*, 3679.
(11) Brown, W. E.; Lehr, J. R.; Smith, J. P.; Frazier, A. W. *J. Am. Chem. Soc.* **1957**, *79*, 5318.
(12) Termine, J. D.; Posner, A. S. *Science* **1966**, *153*, 1523.
(13) Crane, N. J.; Popescu, V.; Morris, M. D.; Steenhuis, P.; Ignelzi, M. A., Jr. *Bone* **2006**, *39*, 434.
(14) Mahamid, J.; Aichmayer, B.; Shimoni, E.; Ziblat, R.; Li, C.; Siegel, S.; Paris, O.; Fratzl, P.; Weiner, S.; Addadi, L. *Proc. Natl. Acad. Sci. U. S. A.* **2010**, *107*, 6316.
(15) Posner, A. S. *Physiol. Rev.* **1969**, *49*, 760.
(16) Elliott, J. C. *Structure and chemistry of the apatites and other calcium orthophosphates*; Elsevier: Amsterdam, 2013; Vol. *18*.
(17) Mahamid, J.; Sharir, A.; Gur, D.; Zelzer, E.; Addadi, L.; Weiner, S. *J. Struct. Biol.* **2011**, *174*, 527.
(18) Omelon, S.; Georgiou, J.; Henneman, Z. J.; Wise, L. M.; Sukhu, B.; Hunt, T.; Wynnyckyj, C.; Holmyard, D.; Bielecki, R.; Grynpas, M. D. *PLoS One* **2009**, *4*, e5634.
(19) Bennet, M.; Akiva, A.; Faivre, D.; Malkinson, G.; Yaniv, K.; Abdelilah-Seyfried, S.; Fratzl, P.; Masic, A. *Biophys. J.* **2014**, *106*, L17.
(20) Spevak, L.; Flach, C. R.; Hunter, T.; Mendelsohn, R.; Boskey, A. *Calcif. Tissue Int.* **2013**, *92*, 418.
(21) Wu, Y.; Glimcher, M. J.; Rey, C.; Ackerman, J. L. *J. Mol. Biol.* **1994**, *244*, 423.
(22) Wu, Y.; Ackerman, J.; Strawich, E.; Rey, C.; Kim, H.-M.; Glimcher, M. *Calcif. Tissue Int.* **2003**, *72*, 610.
(23) Rey, C.; Lian, J.; Grynpas, M.; Shapiro, F.; Zylberberg, L.; Glimcher, M. J. *Connect. Tissue Res.* **1989**, *21*, 267.
(24) Francis, M. D.; Webb, N. C. *Calcif. Tissue Res.* **1970**, *6*, 335.
(25) Habraken, W. J.; Tao, J.; Brylka, L. J.; Friedrich, H.; Bertinetti, L.; Schenk, A. S.; Verch, A.; Dmitrovic, V.; Bomans, P. H.; Frederik, P. M.; et al. *Nat. Commun.* **2013**, *4*, 1507.
(26) Akiva, A.; Malkinson, G.; Masic, A.; Kerschnitzki, M.; Bennet, M.; Fratzl, P.; Addadi, L.; Weiner, S.; Yaniv, K. *Bone* **2015**, *75*, 192.
(27) Sauer, G. R.; Zunic, W. B.; Durig, J. R.; Wuthier, R. E. *Calcif. Tissue Int.* **1994**, *54*, 414.
(28) Fowler, B. O.; Markovic, M.; Brown, W. E. *Chem. Mater.* **1993**, *5*, 1417.
(29) McElderry, J. D. P.; Zhao, G.; Khmaladze, A.; Wilson, C. G.; Franceschi, R. T.; Morris, M. D. *J. Bone Miner. Res.* **2013**, *28*, 1846.
(30) Mandair, G. S.; Morris, M. D. *BoneKEy Rep.* **2015**, *4*, 620.
(31) Avraham-Davidi, I.; Ely, Y.; Pham, V. N.; Castranova, D.; Grunspan, M.; Malkinson, G.; Gibbs-Bar, L.; Mayseless, O.; Allmog, G.; Lo, B.; Warren, C. M.; Chen, T. T.; Ungos, J.; Kidd, K.; Shaw, K.; Rogachev, I.; Wan, W.; Murphy, P. M.; Farber, S. A.; Carmel, L.; Shelness, G. S.; Iruela-Arispe, M. L.; Weinstein, B. M.; Yaniv, K. *Nat. Med.* **2012**, *18*, 967.
(32) Westerfield, M. *Zebrafish Book*; University of Oregon Press: Eugene, OR, 2000; p 4.
(33) Lister, J. A.; Robertson, C. P.; Lepage, T.; Johnson, S. L.; Raible, D. W. *Development* **1999**, *126*, 3757.
(34) Benecke, G.; Wagermaier, W.; Li, C.; Schwartzkopf, M.; Flucke, G.; Hoerth, R.; Zizak, I.; Burghammer, M.; Metwalli, E.; Müller-Buschbaum, P.; Trebbin, M.; Förster, S.; Paris, O.; Roth, S. V.; Fratzl, P. *J. Appl. Crystallogr.* **2014**, *47*, 1797.

DOI: 10.1021/jacs.6b09442
J. Am. Chem. Soc. 2016, 138, 14481−14487